Unveiling the electrolyte effects of CO2 electroreduction to CO and H2 evolution from the interfacial pH perspective

Liu, X.

Chapter 2

Interfacial pH measurements using a Rotating Ring-Disc Electrode with a voltammetric pH sensor

Abstract

Electrochemical reactions in which H^+ or OH^- ions are produced or consumed, affect the pH near the electrode surface. Probing the pH locally is therefore highly desired to understand and model the reaction environment under operando conditions. We carried out interfacial pH measurements under mass transport control using a rotating ring-disc electrode (RRDE) coupled with our recently developed voltammetric pH sensor. The interfacial disc pH is detected by functionalizing the gold ring with a hydroxylaminothiophenol (4-HATP)/4-nitrosothiophenol (4-NSTP) redox couple. As protons only have to interact with a monolayer containing the 4-HATP/4-NSTP, the sensitivity and time resolution that can be achieved are superior to potentiometric sensors. We used hydrogen evolution as a model reaction and performed measurements in buffered and unbuffered electrolytes. The effects of the current density, potential, the buffer capacity of the electrolyte and rotation rate on the local pH were investigated. This work shows a reliable and sensitive method for accurately probing the reaction environment under well-defined mass transport conditions, over a wide pH range.

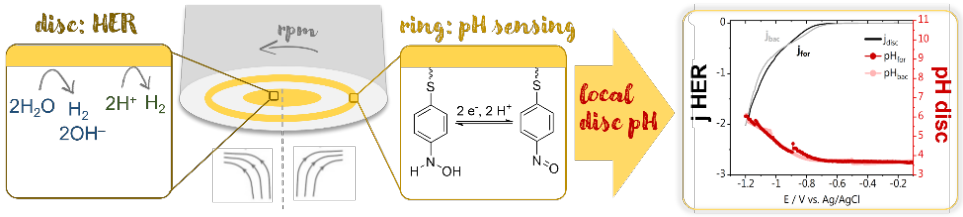

This chapter is based on Monteiro, M. C. O.; Liu, X.; Hagedoorn, B. J. L.; Snabilié, D. D.; Koper, M. T. M., Interfacial pH Measurements Using a Rotating Ring-Disc Electrode with a Voltammetric pH Sensor. ChemElectroChem 2021, 9 (1), e202101223.

2.1 Introduction

Electrochemical reactions that consume/produce protons or hydroxyl ions can generate a pH gradient between the electrode surface and the bulk of the electrolyte. In general, the value of the local pH developed at the surface is a function of the current drawn, the electrolyte composition, and the mass transport conditions.[1] It has been shown that the (local) electrolyte pH plays a significant role in various reactions, such as hydrogen evolution[2] (HER), CO_2 reduction[3], oxygen evolution[4] and reduction[5], among others. Therefore, it is highly desired to probe the pH gradient near the surface during these electrochemical reactions, with high sensitivity, and with good time and spatial resolution.

We have recently reviewed the main techniques available for performing local pH measurements[1], the most frequently used ones being Scanning Electrochemical Microscopy (SECM)[6–8], Scanning Ion Conductance Microscopy (SICM)[9,10], Scanning Ion Selective Electrode (SIET), Rotating Ring-Disc Electrode (RRDE)[11–14], confocal fluorescence scanning microscopy[15], infra-red[16,17] and Raman spectroscopy.[18] Among these, RRDE is the only technique that allows for measurements to be performed under well-defined mass transport conditions, at the expense of the in-plane spatial resolution. Firstly introduced by Albery and Calvo[19–21], pH measurements using RRDE consist of a reaction taking place at the disc electrode and the detection of the proton concentration during the course of this reaction by a pH sensing material at the ring electrode. Due to the electrode geometry and rotation, the flow of species going from the disc to the ring is described by a convective-diffusion equation. This allows the interfacial pH observed at the ring electrode to be directly converted into the pH at the surface of the disc electrode. The advantage is that the detection by the ring electrode does not affect the reactions taking place on the disc electrode. The analytical solution derived by Albery and Calvo[19–21] was recently further developed by Yokoyama et al.[22] by including the autoprotolysis of water in the description, which allows for determining the interfacial disc pH more accurately in a wider pH range.

A few works on interfacial pH measurements with RRDE have been reported, however mainly potentiometric pH sensors were employed, the most common being iridium oxide (IrO_x).[11,13,14] The ring electrode is normally modified with an IrO_x film and the pH at the disc is determined based on the Nernstian open circuit potential (OCP) response of the ring. A major drawback of using IrO_x is that the stability and time resolution depend, for example, on the film thickness and pH.[23,24] Besides IrO_x, certain reactions on bare metal surfaces have also been used to estimate changes in local pH. Figueiredo et al.[12] used shifts in the equilibrium potential of the hydrogen evolution reaction on a Pt ring to estimate the disc pH during ethanol oxidation. Zhang et al. used the CO oxidation reaction on a gold ring to probe the disc pH during CO_2 reduction to CO on gold.[13] However, it is known that the sensitivity

and accuracy of these measurements can be highly compromised by the reaction environment, as both HER and CO oxidation have shown to be affected, i.e. by the cation[25–27], surface structure[28,29] and pH.[30,31] Also, buffering species in the electrolyte are not always taken into account when converting the pH measured at the ring to the local disc pH, which may lead to an overestimation of the local alkalinity. Besides that, based on the analytical description of Yokoyama et al.[22], changes of the local disc pH may correspond to an order of magnitude smaller changes in the ring pH based on detection efficiency and buffering, especially in solutions far from neutral pH. Therefore, a more sensitive pH sensor for RRDE is desired, and in fact necessary, for performing accurate interfacial pH measurements with this technique.

In this work, we have assessed the feasibility of using our previously developed voltammetric pH sensor in the RRDE configuration. The sensor consists of a self-assembled monolayer on gold, and was previously used for local pH measurements in the diffusion layer with SECM.[32,33] The pH response is based on the voltammetry of the hydroxylaminothiophenol (4-HATP)/4-nitrosothiophenol (4-NSTP) redox couple, specifically the Nernstian shift of the oxidation reaction mid-peak potential. We show here that the 4-HATP/4-NSTP voltammetric response is not affected by the electrode rotation, and that this redox couple can be used in a RRDE system. We employed it to probe the interfacial disc pH during hydrogen evolution in buffered and unbuffered electrolytes at mildly acidic pH. With the high sensitivity and time resolution of this voltammetric sensor, we measured the interfacial disc pH during cyclic voltammetry, chronoamperometry and chronopotentiometry experiments, and also determined the rotation rate required to minimize interfacial pH changes in the electrolytes studied. The application of this sensitive and reliable pH sensor for RRDE pH measurements presents an alternative to commonly used potentiometric sensors, and a step forward to more accurately probing the reaction environment under well-defined mass transport conditions.

2.2 Experimental Section

Materials. All glassware used was cleaned by immersion in a potassium permanganate solution overnight (1 g/L $KMnO_4$ dissolved in 0.5 M H_2SO_4), followed by immersion in dilute piranha. The glassware was further boiled in ultrapure water at least five times. The electrolytes used in this work, KH_2PO_4 (Alfa Aesar, dried, 99.99 %) and K_2SO_4 (Alfa Aesar, Puratronic, 99.997 %, metals basis), were adjusted to pH 3-5 by addition of appropriate amounts of H_2SO_4 (Merck, Suprapur, 96%) or H_3PO_4 (ortho-Phosphoric acid 85%, Suprapur®, Merck).

pH sensor fabrication and characterization. A gold ring electrode (E6R1PK tip, Pine Research Instrumentation) was used in this work, together with a gold disc (diameter = 5 mm, Pine Research Instrumentation). Prior to experiments, the ring and the disc (Pine Research Instrumentation) were polished with a polycrystalline diamond suspension of 0.25 µm (MetaDi, Buehler) and then sonicated (Bandelin Sonorex RK 52H) in ultrapure water (>18.2 MΩ cm, Millipore Milli-Q) for 10 minutes.[36] Before functionalization of the ring with the pH sensing monolayer, the ring and disc were characterized by recording the blank voltammetry between 0.1 and 1.75 V vs. RHE in argon saturated (6.0 purity, Linde) 0.1 M H_2SO_4 (Merck, Suprapur, 96%) in a one compartment electrochemical cell. A gold wire (0.5 mm diameter, MaTeck, 99.9%) was used as counter electrode and a reversible hydrogen electrode (RHE) as reference. The electrochemically active surface area (ECSA) of the disc was calculated based on the charge corresponding to the gold oxide reduction and a specific capacitance of 386 µC/cm^2.[37] The gold ring electrode is modified by immersing it (without the disc inserted) into a 1 mM solution of 4-NTP (Merck, 80%) in ethanol for 15 minutes. The ring is then thoroughly rinsed with ethanol and water, and dried. The disc electrode is carefully inserted in the shaft, avoiding too much friction (which could damage the 4-NTP monolayer). The 4-NTP is then electrochemically reduced to 4-HATP in the working electrolyte (pH ≈ 4) by cycling the ring from 0.3 to -0.43 V vs. Ag/AgCl (argon saturated, 100 mV s^{-1}). It is important to point out that the monolayer can be easily removed from the gold ring by polishing it with a polycrystalline diamond suspension of 0.25 µm. This can be done whenever necessary i.e. when the 4-HATP/4-NSTP signal is for some reason compromised. A decrease in signal can be caused e.g., by bubbles and loss of potential control during measurements. Considering how simple and fast the pH sensor synthesis is, it is advised to always have a fresh monolayer adsorbed onto the surface at the start of new experiments.

RRDE pH measurements. All electrochemical measurements were carried out using a BioLogic 2-channel potentiostat/galvanostat/ EIS (SP-300). The ring and disc electrodes were controlled simultaneously, by two different potentiostat channels. Two gold wires (0.5 mm diameter, MaTeck, 99.9%) were used as counter electrodes and a Ag/AgCl (low profile, BioLogic) as reference. Argon (6.0 purity, Linde) was purged through the solution for 20 minutes prior to the experiments. The argon flow was kept also during the experiments in order to avoid oxygen diffusing into the electrolyte. The ring cyclic voltammetry (CV) was constantly recorded at 200 mV/s while hydrogen evolution took place at the disc.

Calculating the local disc pH. The mid-peak potential (E_{peak}) of the 4-HATP oxidation to 4-NSTP was determined by fitting the forward scans with a Gaussian function containing a linear background. E_{peak} was then converted to the ring pH (pH_{ring}) using the calibration curve of the 4-HATP/4-NSTP from our previous work: $pH_{ring} = (0.341 - E_{peak})/0.057$.[32] It is

important to point out that the ring open circuit potential (OCP) cannot be used to extract the ring pH, as the 4-NTP monolayer initially adsorbed to the gold is only partially converted to the 4-HATP/4-NSTP redox couple, yielding a convoluted OCP response. To calculate the interfacial disc pH (pH_{disc}), for an unbuffered electrolyte, we use Equation 1, from Yokoyama et al.[22], which is an extension of the analytical solution of Albery and Calvo[19,20], taking the autoprotolysis of water (Equation 2) into account.

$$c_{r,H^+} - c_{r,OH^-} = N_D\left(c_{d,H^+} - c_{d,OH^-}\right) + (1 - N_D)\left(c_{\infty,H^+} - c_{\infty,OH^-}\right) \quad (1)$$

$$K_W = c_{rt,H^+} c_{rt,OH^-} \quad (2)$$

c_∞ represents the proton or OH^- concentration in the bulk and $c_{d,}$ and $c_{r,}$ the same at the disc and ring, respectively. The detection efficiency N_D is given by Equation S3 and S4 (see Supporting Information) and is only dependent on the geometrical parameters of the ring and disc electrode, see Figure S1. For the electrode used in this work N_D = 0.23. Figure S2 in the Supporting Information (SI) shows the theoretical relationships between pH_{Disc} and pH_{Ring} at various pH_∞, comparing Equation 1 (Yokoyama) and Equation S1 (Albery and Calvo) for an unbuffered electrolyte. It can be observed that not taking the

autoprotolysis of water into account can lead to over/underestimating the disc pH, depending on the bulk pH. Equation 1 was rewritten as follows and used to convert pH_{ring} to pH_{disc}.

$$pH_{disk} = -\log\left(\frac{c_{r,H^+} - c_{rt,OH^-}}{N_D} - \frac{c_{\infty,H^+} - c_{\infty,OH^-}}{N_D} + c_{\infty,H^+} - c_{\infty,OH^-}\right) \quad (3)$$

For buffered systems, as the phosphate electrolyte used in this work, a correction must be applied to Equation 3, to consider the homogeneous reactions taking place involving the phosphate species. In this case, the OH^- concentration is given by Equation 4 and is applied to Equation 5 to obtain the interfacial disc pH.

$$c'_{OH^-} = c_{OH^-} + [H_2PO_4^-] + 2\ [HPO_4^{2-}] + 3\ [PO_4^{3-}] \quad (4)$$

$$N_D = \frac{c'_{r,OH^-} - c'_\infty}{c'_{d,OH^-} - c'_\infty} \quad (5)$$

The equilibrium constants and further details are available in the Supporting Information, Equations S5-S14. The analytical solution of the quartic equation that results, is shown in Equations S15-S24. The theoretical relationship between pH_{Disc} and pH_{Ring} at various pH_∞ for a phosphate buffered system is shown in Figure S2c in the SI.

2.3 Results and Discussion

Interfacial pH measurements during hydrogen evolution (HER) using a rotating ring-disc

electrode (RRDE) were performed using the electrode assembly schematically represented in Figure1a. Prior to measurements, the gold ring and disc electrodes are characterized by blank voltammetry, to assure a clean and reproducible surface (see Figure S3a in the Supporting Information (SI)). For the pH sensing, the gold ring is modified with a self-assembled monolayer of 4-NTP, which is then electrochemically converted to the 4-HATP/4-NSTP redox couple by cyclic voltammetry, as shown in Figure1b. The 4-NTP modified gold ring is immersed in the electrolyte under potential control (0.3 V vs. Ag/AgCl) and then a cathodic sweep at 100 mVs^{-1} is performed to partially reduce the monolayer to 4-HATP. The voltammetry of the resulting 4-HATP/4-NSTP redox couple is also shown in Figure1b recorded at 200 mVs^{-1} (in red), which is the scan rate used during the pH measurements. In principle, even higher scan rates can be used (up to 500 mVs^{-1}), if the process being studied

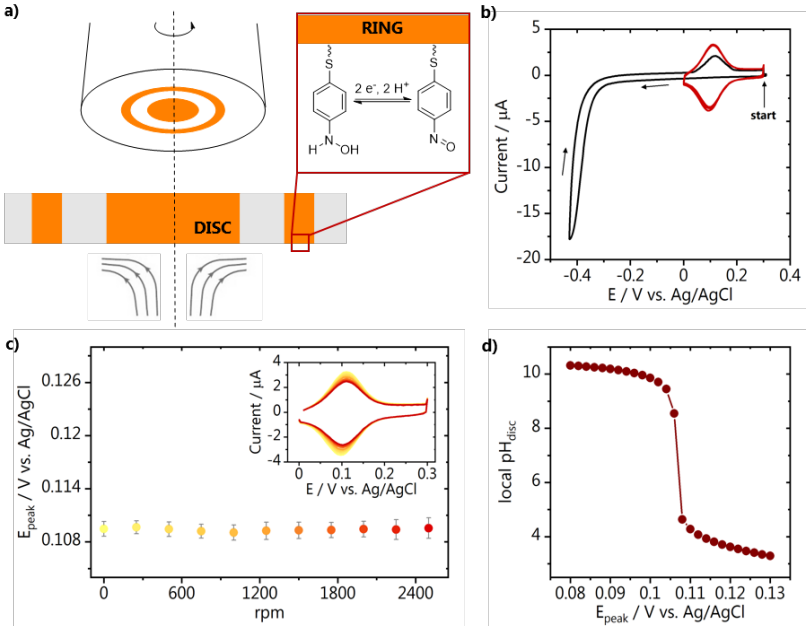

Figure 1. a) Schematic representation of the RRDE with the functionalized ring; b) cyclic voltammetry of the 4-NTP to 4-HATP conversion (black, 100 mV s–1) together with a characterization of the 4-HATP/4-NSTP redox couple (red, 200 mV s^{-1}). Both were recorded in 0.1 M K_2SO_4, pH = 4. c) Effect of rotation on the pH sensor mid-peak potential, extracted from the voltammograms shown in the inset. d) Theoretical relationship between E_{peak} and pH_{disc} using Equation 1 for $pH_\infty = 4$.

requires better time resolution. Different from our previous work, here the molecule conversion was performed in the same electrolyte as in which HER was carried out. We find

that it gives similar results as in the previously used 0.1 M H_2SO_4 if the 60 mV/pH Nernstian shift of the potential window is taken into account. We show here the voltammetry for the conversion in 0.1 M K_2SO_4 at pH = 4 (Figure1b). In Figure S3b in the SI, the same is shown in 0.1 KH_2PO_4 and 0.1 M H_2SO_4, for comparison. The molecule conversion has also been successfully performed in, for example, perchlorate and bicarbonate electrolytes, although not shown here.

Before performing the interfacial pH measurements, we have investigated if the rotation of the electrode has any influence on the 4-HATP/4-NSTP response. The ring voltammetry (CV)

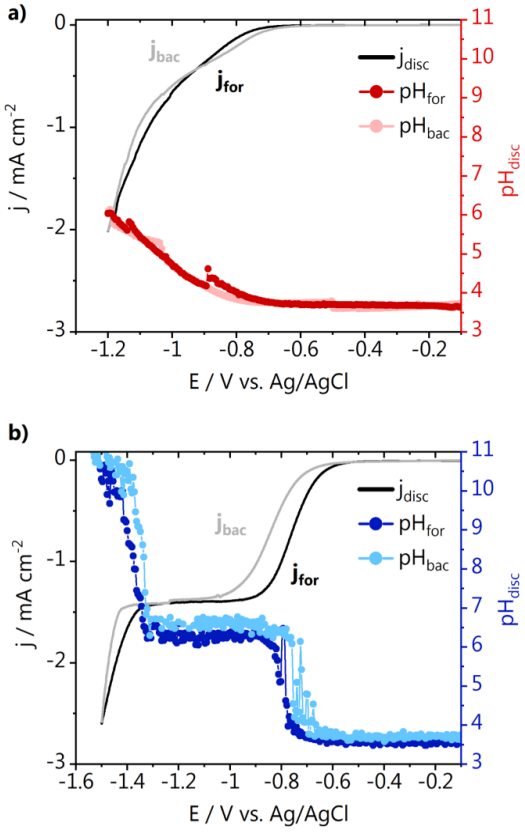

Figure 2. Interfacial pH measurement during the disc cyclic voltammetry in 0.1 M argon saturated at 2000 rpm in a) KH_2PO_4 pH_{bulk} = 3.7 and b) K_2SO_4 pH_{bulk} = 3.5. CVs were recorded at 2 mV s^{-1} and the 4-HATP/4-NSTP CVs at 200 mV s^{-1}. The forward and backward scans are indicated as j_{for}, pH_{for} and j_{bac}, pH_{bac}.

was constantly recorded while the rotation rate was varied. Results are shown in Figure1c going from 0 to 2600 rpm. Each data point is the average mid-peak potential (E_{peak}) determined from 10 consecutive cycles together with the standard deviation, and the corresponding CVs are shown in the graph inset. We observe a stable E_{peak} of 0.109 V vs. Ag/AgCl for all rotation rates. There is a slight decrease in the absolute ring current, however this does not affect the peak fitting and extraction of E_{peak}. These results assure that any changes in the ring voltammetry during HER are due to the reaction taking place at the disc, and not affected by the rotation rate or the turbulence of the electrolyte. This is very important, especially when working far from neutral pH. As shown in Figure1d, considering an unbuffered electrolyte with a bulk pH of 4, a difference of 20 mV in E_{peak} corresponds to a change in pH_{disc} of 7 pH units. The entire E_{peak} range plotted is actually only 50 mV, which

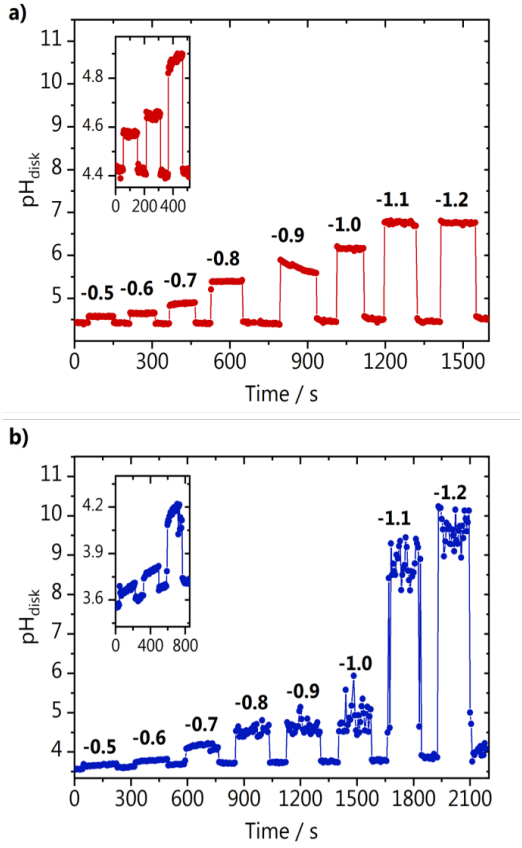

Figure 3. Interfacial pH measurement during chronoamperometry (potentials indicated in the graph in V vs. Ag/AgCl) in 0.1 M argon saturated a) KH_2PO_4 pH_{bulk} = 4.4 and b) K_2SO_4 pH_{bulk} = 3.6 at 1600 rpm.

corresponds to the detection of a change of less than a unit in the local ring pH. This also indicates how important it is that the pH sensor employed for RRDE measurements is sensitive and stable enough, to measure the local pH accurately.

We employed the modified ring electrode to measure the development of the interfacial pH during a cyclic voltammogram on the gold disc. Hydrogen evolution was carried out in phosphate and sulfate electrolyte and the correlation between the current density and the measured surface disc pH can be seen in Figure 2 a and Figure 2b, respectively. It is important to point out that the conversion from the measured ring pH to the disc pH is done differently for the experiment in unbuffered sulphate electrolyte in comparison to the phosphate buffer. For sulphate, the analytical description of Yokoyama et al.[22] is used. In the case of phosphate, we add a correction to account for the homogeneous reactions involving the different phosphate species ($H_2PO_4^-, HPO_4^{2-}, PO_4^{3-}$) that take place upon increase in the local alkalinity (see the section "Calculating the local disc pH" in the Experimental Section). In Figure 2, we observe that the pH profiles are nearly a mirror image of the current density in both phosphate and sulphate electrolytes. In Figure 2a, we see a gradual increase in current and local pH from 0 to –0.9 V vs. Ag/AgCl. At more negative potentials there is steeper increase in current, likely due to the transition from proton reduction to water and biphosphate reduction as the main branch of HER taking place.[34] Despite the high current, the interfacial disc pH does not go above 6, due to the buffer capacity of the phosphate electrolyte used. In sulphate electrolyte (Figure 2b) a more well-defined plateau is present due to diffusion limited proton reduction ($2H^+ + 2e^- \rightarrow H_2$) followed by a steep increase in current due to water reduction ($2H_2O + 2e^- \rightarrow H_2 + 2OH^-$). The activity for proton reduction starts to increase at about –0.55 V vs. Ag/AgCl and a consequent increase in the interfacial disc pH starts to be observed from –0.57 V vs. Ag/AgCl onwards. This slight delay of 20 mV in the pH response in comparison to the current response is likely because at the very low overpotentials the reaction is only limited by the rate of charge transfer at the electrode-solution interface and there are no pronounced changes in the local proton concentration. At potentials more negative than –0.57 V vs. Ag/AgCl a combination of charge and mass transfer processes control the reaction, and the interfacial pH starts increasing. In the potential window in which the diffusion limited proton reduction plateau is observed, the local disc pH remains around 6.5, until the activity for water reduction increases and consequently the interfacial pH gradually becomes more alkaline. The differences in activity between phosphate and sulphate electrolyte are likely due to the fact that it has been shown that phosphate can outcompete water as a proton donor for hydrogen evolution.[34] We see that due to the high time resolution achieved with

the 4-HATP/4-NSTP sensor in combination with the low scan rate of the CV (2 mV s^{-1}), detailed information regarding the correlation between current and pH can be obtained. In principle, the disc voltammetry can also be recorded at higher scan rates, at the expense of the resolution of the pH measurement.

Next, we have performed interfacial pH measurements while applying different potentials to the disc electrode. In between potential steps, HER was turned "off" by applying 0 V vs. Ag/AgCl to the disc and the ring voltammetry was constantly recorded. The current and potential recorded in time can be seen in Figure S4 in the SI. Results are shown in Figure 3 for HER carried out in phosphate and sulphate electrolyte. The increase in interfacial disc pH as a function of potential here is slightly larger than what was observed for the cyclic voltammetry from Figure 2. This is due to the lower rotation rate (1600 rpm) employed during the chronoamperometry, slowing down the transport of species away from the electrode surface. At the low overpotentials, we can accurately detect differences in local pH as small as 0.1 pH unit, which has not been previously reported for RRDE pH measurements. This is due to the better sensitivity of the 4-HATP/4-NSTP redox couple used in this work compared to the commonly used pH sensors. The insets in Figure 3a and Figure 3b show the pH measured at –0.5, –0.6 and –0.7 V vs. Ag/AgCl, and highlight how the interfacial pH in the phosphate electrolyte always returns to the bulk pH value once the reaction is turned "off". The same does not happen in sulphate, where the baseline keeps increasing due to the lower buffer capacity of the electrolyte. The phosphate electrolyte has different strong buffering regions, namely at pH values around the pK_a of the following reversible reactions: $H_3PO_4 \leftrightarrow H_2PO_4^-$ (pK_a = 2.3), $H_2PO_4^- \leftrightarrow HPO_4^{2-}$ (pK_a = 7.2) and $H_2PO_4^- \leftrightarrow PO_4^{3-}$ (pKa = 12.1). In contrast, in the sulfate electrolyte, only one equilibrium reaction is present ($HSO_4^- \leftrightarrow SO_4^{2-}$) with pK_a = 1.8, considerably lower than the pH developed during HER. It is important to point out that fluctuations of the pH response as observed, for example, at large overpotentials in Figure 3b, occur due to bubbles accumulating near the ring electrode. Even though in this work this did not compromise the measurements, for more challenging systems (or working conditions) this can be circumvented by coating the spacer that separates the ring and the disc electrodes with dopamine.[35]

The buffer capacity of the electrolyte, the current density, and especially the rotation rate, determine the magnitude of the pH gradients developed during RRDE experiments. Therefore, we have also probed to which extent enhancing mass transport affects the interfacial disc pH by performing chronopotentiometry measurements in the same phosphate and sulphate electrolytes. The reaction was turned "on" and "off" by applying a constant current density of –0.4 mA cm^{-2} or –0.001 mA cm^{-2} to the disc, at different rotation rates (see Figure S5 in the SI for the current and potential recorded). Figure 4 a shows the

interfacial disc pH during HER in phosphate electrolyte at different rotation rates. Although the changes in pH are not drastic, we see that between 500 and 1000 rpm, the convective flow of species is not high enough to avoid a larger increase in the local alkalinity, despite the buffer capacity of the electrolyte. Still, the interfacial pH when HER is "on" decreases by increasing the rotation rate. At rotations higher than 1250 rpm, a steady state is reached, i.e. the highest flux of species outwards is achieved and increasing rotation no longer decreases the local alkalinity. This happens because a maximum efficiency at which species move from the disc to the ring is reached, as also discussed in the work of Zimer et al.[11] Due to the buffering species in the phosphate electrolyte, which have easier access to the surface at the higher rotations, the interfacial disc pH in phosphate equilibrates at values

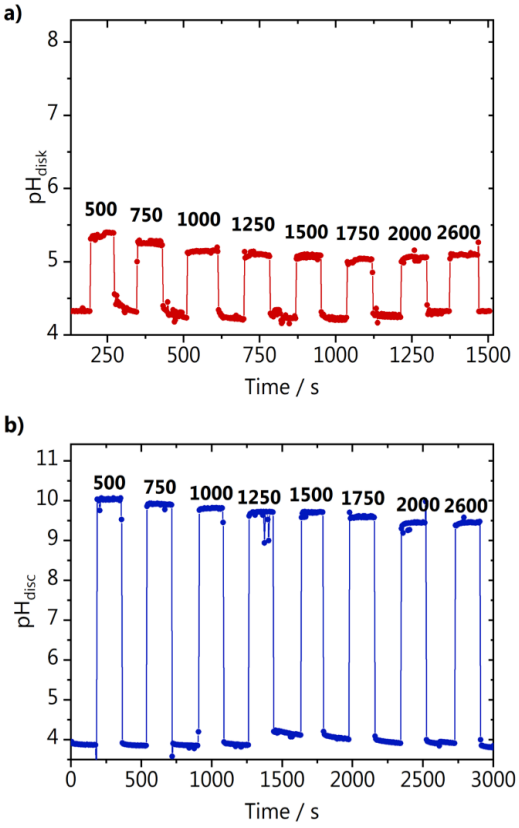

Figure 4. Interfacial pH measurements during chronopotentiometry (constant current density = –0.42 mA cm^{-2}) in 0.1 M argon saturated a) KH_2PO_4 pH_{bulk} = 4.4 and b) K_2SO_4 pH_{bulk} = 4.0 at the different rotations indicated in the graph in rpm.

around 5.2 at steady state. A different behaviour is observed in the sulphate electrolyte (Figure 4b). Here, although increasing rotation also gradually decreases the local disc pH, a stable pH is never reached at high rotation rates, due to the low buffer capacity of the electrolyte. Additionally, the interfacial disc pH never returns to the bulk value when the reaction is turned "off" (in between different rotations), similarly to what we observed in the chronoamperometry experiment in sulphate (inset of Figure 3b). It is important to point out that even though the calculated interfacial disc pH changes are relatively large, the differences in E_{peak} recorded at the ring electrode are rather small. Figure S6 in the SI exemplifies that with the E_{peak} recorded for the experiments shown in Figure 4. The changes in E_{peak} observed during the whole experiment are in the 15-40 mV range, highlighting once more how important it is to employ a sensitive pH sensor for RRDE pH measurements.

The results shown demonstrate that, even though RRDE systems are used to avoid (or minimize) concentration gradients during electrochemical reactions, the effectiveness of the enhancement in mass transport is highly dependent on the electrolyte buffer capacity and on the currents drawn. Assuming "well-defined mass transport conditions" when working with RRDE does therefore not imply absence of concentration gradients, as we see that (in our working conditions) the local disc pH can vary up to 6-7 pH units from the bulk pH. This has important consequences, for example, for measurements performed as a function of rotation rate going from low to high rotations. The local pH values will be significantly different, and their effect is difficult to deconvolute, unless proper quantification of the pH is carried out. In the electrolytes studied, even with a relatively high buffer capacity (phosphate electrolyte) and rotation rates (> 1250 rpm), the interfacial disc pH differed by 1 unit from the bulk. Operating in the steady state regime (strong buffer, high rotations) minimizes convoluted responses due to differences in the interfacial disc pH. However, as evidenced by our results, this regime is strongly dependent on the electrolyte and reaction activity, and has to be identified for each individual system studied. Using the 4-HATP/4-NSTP redox couple as pH sensor on the ring electrode, allows to do so with high temporal resolution and sensitivity. The synthesis of the functionalized gold ring shown in this work is much simpler than what was previously reported for IrOx[11], highly reproducible, and the system is versatile in terms of disc materials that can be employed, and reactions to be studied.[33] Finally, even though the analytical description from Albery and Calvo[19–21] and Yokoyama et al.[22] is accurate for calculating pH_{disc} for measurements performed in unbuffered electrolytes, here we present a method to correct the description when working in buffered solutions. This is crucial to avoid an overestimation of the interfacial disc pH in buffered systems.

2.4 Conclusion

In this work we have shown that RRDE interfacial pH measurements can be performed with high sensitivity and temporal resolution using a voltammetric pH sensor. A gold ring functionalized with the 4-HATP/4-NSTP redox couple has been used to study pH gradients developing during hydrogen evolution at a gold disc electrode. The interfacial disc pH is measured in phosphate or sulphate electrolyte during different electrochemical experiments: cyclic voltammetry, chronoamperometry and chronopotentiometry. We observed that the changes in interfacial pH at the disc strongly depend on the buffer capacity of the electrolyte and the current drawn (i.e. the activity). By varying the rotation rate at constant current density, we identify the minimum rotation required to achieve the maximum enhancement of mass transport possible and avoid strong concentration gradients during the electrocatalytic measurements. Using HER as a model system, we show that the 4-HATP/4-NSTP voltammetric pH sensor is a powerful tool for accurately measuring interfacial pH with RRDE, with high time resolution.

References

[1] M. C. O. Monteiro, M. T. M. Koper, *Curr. Opin. Electrochem.* **2021**, *25*, 100649.

[2] A. Goyal, M. T. M. Koper, *Angew. Chemie Int. Ed.* **2021**, *60*, 13452–13462.

[3] Z. Zhang, L. Melo, R. P. Jansonius, F. Habibzadeh, E. R. Grant, C. P. Berlinguette, *ACS Energy Lett.* **2020**, *5*, 3101–3107.

[4] L. Giordano, B. Han, M. Risch, W. T. Hong, R. R. Rao, K. A. Stoerzinger, Y. Shao-Horn, *Catal. Today* **2016**, *262*, 2–10.

[5] M. F. Li, L. W. Liao, D. F. Yuan, D. Mei, Y.-X. Chen, *Electrochim. Acta* **2013**, *110*, 780–789.

[6] M. C. O. Monteiro, L. Jacobse, T. Touzalin, M. T. M. Koper, *Anal. Chem.* **2020**, *92*, 2237–2243.

[7] C. S. Santos, A. S. Lima, D. Battistel, S. Daniele, M. Bertotti, *Electroanalysis* **2016**, *28*, 1441–1447.

[8] S. Dieckhöfer, D. Öhl, J. R. C. Junqueira, T. Quast, T. Turek, W. Schuhmann, *Chem. – A Eur. J.* **2021**, *27*, 5906–5912.

[9] B. P. Nadappuram, K. McKelvey, R. Al Botros, A. W. Colburn, P. R. Unwin, *Anal. Chem.* **2013**, *85*, 8070–8074.

[10] C. A. Morris, C. C. Chen, T. Ito, L. A. Baker, *J. Electrochem. Soc.* **2013**, *160*, H430–H435.

[11] A. M. Zimer, M. Medina da Silva, E. G. Machado, H. Varela, L. H. Mascaro, E. C. Pereira, *Anal. Chim. Acta* **2015**, *897*, 17–23.

[12] M. C. Figueiredo, R. M. Arán-Ais, V. Climent, T. Kallio, J. M. Feliu, *ChemElectroChem* **2015**, *2*, 1254–1258.

[13] F. Zhang, A. C. Co, *Angew. Chemie - Int. Ed.* **2020**, *59*, 1674–1681.

[14] P. Steegstra, E. Ahlberg, *J. Electroanal. Chem.* **2012**, *685*, 1–7.

[15] A. J. Leenheer, H. A. Atwater, *J. Electrochem. Soc.* **2012**, *159*, H752–H757.

[16] K. Yang, R. Kas, W. A. Smith, *J. Am. Chem. Soc.* **2019**, *141*, 15891–15900.

[17] O. Ayemoba, A. Cuesta, *ACS Appl. Mater. Interfaces* **2017**, *9*, 27377–27382.

[18] D. A. Henckel, M. J. Counihan, H. E. Holmes, X. Chen, U. O. Nwabara, S. Verma, J. Rodríguez-López, P. J. A. Kenis, A. A. Gewirth, *ACS Catal.* **2021**, *11*, 255–263.

[19] W. J. Albery, E. J. Calvo, *J. Chem. Soc. Faraday Trans. 1 Phys. Chem. Condens. Phases* **1983**, *79*, 2583–2596.

[20] W. J. Albery, A. R. Mount, *J. Chem. Soc. Faraday Trans. 1 Phys. Chem. Condens. Phases* **1989**, *85*, 1181.

[21] W. J. Albery, A. R. Mount, *J. Chem. Soc. Faraday Trans. 1 Phys. Chem. Condens. Phases* **1989**, *85*, 3717.

[22] Y. Yokoyama, K. Miyazaki, Y. Miyahara, T. Fukutsuka, T. Abe, *ChemElectroChem* **2019**, 4750–4756.

[23] P. Steegstra, E. Ahlberg, *Electrochim. Acta* **2012**, *76*, 26–33.

[24] A. J. Bard, M. V. Mirkin, *Scanning Electrochemical Microscopy*, CRC Press, **2012**.

[25] X. Chen, I. T. McCrum, K. A. Schwarz, M. J. Janik, M. T. M. Koper, *Angew. Chemie - Int. Ed.* **2017**, *56*, 15025–15029.

[26] G. García, *ChemElectroChem* **2017**, *4*, 459–462.

[27] S. Xue, B. Garlyyev, S. Watzele, Y. Liang, J. Fichtner, M. D. Pohl, A. S. Bandarenka, *ChemElectroChem* **2018**, *5*, 2326–2329.

[28] P. Rodriguez, M. T. M. Koper, *Phys. Chem. Chem. Phys.* **2014**, *16*, 13583–13594.

[29] G. García, M. T. M. Koper, *ChemPhysChem* **2011**, *12*, 2064–2072.

[30] H. Kita, K. Shimazu, K. Kunimatsu, *J. Electroanal. Chem.* **1988**, *241*, 163–179.

[31] J. Rossmeisl, K. Chan, E. Skúlason, M. E. Björketun, V. Tripkovic, *Catal. Today* **2016**, *262*, DOI 10.1016/j.cattod.2015.08.016.

[32] M. C. O. Monteiro, L. Jacobse, T. Touzalin, M. T. M. Koper, *Anal. Chem.* **2020**, *92*, 2237–2243.

[33] M. C. O. Monteiro, L. Jacobse, M. T. M. Koper, *J. Phys. Chem. Lett.* **2020**, *11*, 9708–9713.

[34] M. N. Jackson, Y. Surendranath, *J. Am. Chem. Soc.* **2016**, *138*, 3228–3234.

[35] J. G. Vos, M. T. M. Koper, *J. Electroanal. Chem.* **2019**, *850*, 113363.

[36] M. C. O. Monteiro, M. T. M. Koper, *Electrochim. Acta* **2019**, *325*, 134915.

[37] U. P. Do, F. Seland, E. A. Johannessen, *J. Electrochem. Soc.* **2018**, *165*, 219–228.